Direct observation of vortex pinning by dislocations in $Bi_2Sr_2CaCu_2O_8$ single crystals

1995 Supercond. Sci. Technol. 8 605

(http://iopscience.iop.org/0953-2048/8/8/002)

Supercond. Sci. Technol. 8 (1995) 605–612. Printed in the UK

Direct observation of vortex pinning by dislocations in $Bi_2Sr_2CaCu_2O_8$ single crystals

K E Bagnall†, I V Grigorieva†, J W Steeds†, G Balakrishnan‡ and D McK Paul‡

† Physics Department, University of Bristol, Bristol BS8 1TL, UK
‡ Physics Department, University of Warwick, Coventry CV4 7AL, UK

Received 12 April 1995, in final form 6 June 1995

Abstract. A technique allowing simultaneous observation of vortex images and crystal defects in superconductors by transmission electron microscopy (TEM) has been developed. The vortices are visualized by the Bitter decoration method followed by preparation of the samples for TEM. The technique was used to study the effect of crystal dislocations on the flux line lattice (FLL) in single crystals of $Bi_2Sr_2CaCu_2O_8$. Individual dislocations having a local density comparable with that of the vortices are found to cause local disorder in the otherwise well-ordered FLL, acting as attractive pinning centres. We show that the main contribution to pinning in our experiments comes from strain fields around dislocations. Relevant pinning mechanisms are discussed such as those arising from local changes of superconducting parameters caused by the dislocation strain fields or from vortex–dislocation interaction of an elastic nature.

1. Introduction

Crystal dislocations, when present in large numbers, are well known to be effective pinning centres in superconductors. Many studies of conventional low-T_c superconductors have demonstrated that the introduction of dense dislocation tangles into superconducting crystals enhances the bulk pinning force and critical currents by as much as one or two orders of magnitude (for a review, see [1]). At the same time, individual dislocations impose only weak collective pinning on the flux line lattice (FLL) [2, 3]. A number of recent studies on high-T_c copper oxide superconductors have also demonstrated strong correlations between the presence of high densities of dislocations and substantial enhancement of vortex pinning and critical currents in $YBa_2Cu_3O_x$ (YBCO) [4, 5], $Bi_2Sr_2CaCu_2O_8$ (BSCCO) and $(Bi,Pb)_2Sr_2CaCu_2O_8$ [6–8]. Dislocation networks are present naturally in as-grown single crystals of BSCCO [6]. Higher densities of dislocations can be introduced by hot uniaxial compression or hot isostatic pressing [4, 7] or during the solid state reaction process [5, 8].

Concerning pinning by dislocations, at least two questions remain unresolved. First, what is the effect of individual dislocations on the flux line lattice and, second, what is a particular mechanism of interaction between the vortices and the dislocations. Only after the answers to these questions are known, can it become possible to understand fully the effect of a given dislocation density on superconducting characteristics. Such considerations are of particular importance for developing superconducting materials capable of carrying high critical currents or superconducting devices such as those based on grain-boundary Josephson junctions.

Simultaneous observation of dislocation and vortex arrangements is the most obvious way to answer the first of the above questions and also to distinguish between possible mechanisms of the dislocation–vortex interaction. Three basic mechanisms for vortex pinning by dislocations have been proposed. The first is due to local suppression of superconductivity in the vicinity of a dislocation, caused by the dislocation strain field [9]. The other two arise from variations of elastic properties of materials between the normal and superconducting states [10–13]. For the study presented here, we developed a technique that allowed simultaneous observation of vortex positions and crystal dislocations in the transmission electron microscope (TEM). The vortex positions were revealed by the Bitter decoration technique, prior to TEM studies. Our experiments, on as-grown BSCCO-2212 single crystals, demonstrate that crystal dislocations of density comparable with the density of the vortices cause local disorder in the vortex lattice: the vortices are clearly attracted to dislocations of all characters (edge, screw and mixed). Furthermore, the results suggest that the dominant contribution to the vortex–dislocation interaction comes from the strain fields around dislocations.

0953-2048/95/080605+08$19.50

2. Experimental results

Experiments were carried out on high-quality single crystals of BSCCO-2212 grown by the floating zone method using a double ellipsoidal infrared image furnace. Details of the crystal growth are published elsewhere [14]. As-grown crystals were characterized by sharp, ~1–2 K, superconducting transitions and high superconducting transition temperatures, $T_c = 90$–93 K. T_c has been shown to be critically dependent on both the cation concentration and the oxygen concentration [15]. It was found that when annealed in oxygen, the crystals showed deterioration of their superconducting properties which, however, could be recovered by a short anneal in a slightly oxygen-deficient atmosphere. The Bitter decoration technique used to visualize the vortex arrangement is now a standard method used by several groups. It is sensitive to inhomogeneities of the magnetic field created by the vortices at the sample surface. The vortex positions at the surface are 'decorated' by magnetic particles (in our case, Fe particles) producing a snap-shot of the vortex structure at the time of decoration. The method is restricted to low magnetic fields, $H < H_{c1}$, where the vortex spacing, a, is well in excess of the magnetic penetration depth, λ, and the magnetic fields of neighbouring vortices do not overlap. In order to expose fresh crystal surfaces, the samples were cleaved immediately before decoration. Typical sizes of cleaved crystals were $2.5 \times 2.5 \times 0.03$–$0.05$ mm^3. Decoration experiments were performed at 4.2 K in the field-cooling mode, with the magnetic field applied perpendicular to the broad face of the sample ((ab) plane). Here we report the results obtained on two crystals, both decorated in an external field of 40 Oe.

The most straightforward way to combine decoration experiments with TEM observations is first to thin a sample to perforation so that it can be viewed in the transmission microscope and then to decorate it (this procedure was used by Herring [2] to study Nb foils). However, our attempts at such experiments on BSCCO crystals always failed, presumably because of the ease with which overheating can occur at the thin edge of the sample and/or the damage caused to the specimen during ion-milling. Therefore, we have chosen the following procedure. First, the sample was decorated as described above; then, in order to protect the resultant distribution of the magnetic particles (vortex images), a thin (several hundred angstroms) carbon film was deposited on the decorated surface; finally, the sample was ion-milled to perforation from the back. The ion-milling was done in a GATAN ion thinner using 4 kV Ar ions with an incidence angle of 14° and a liquid nitrogen cooled sample holder. The microstructures of the samples together with the vortex images were studied in a Philips EM430 transmission electron microscope operated at an accelerating voltage of 250 kV.

An image of the vortex lattice obtained by scanning electron microscopy (SEM) prior to carbon deposition, and typical for our crystals, is shown in figure 1. The vortices form a homogeneous and well ordered FLL confirming the homogeneity and high quality of the crystals. It should be noted that further manipulations of the samples, in preparation for TEM examination, spoiled somewhat the 'appearance' of the vortex images. In particular, the presence of the carbon film has, in some cases, made the vortex pattern less clear. For comparison, we show two similar pictures of the FLL for sample A taken by SEM without carbon (figure 2(a)) and by TEM with the carbon film in place (figure 2(b)).

Our samples were found to have rather low dislocation densities. Typically, dislocations occupied no more than 5% of the total area of the crystals studied. They were inhomogeneously distributed and concentrated in regions where they formed, sometimes very regular, dislocation networks. Similar dislocation networks have been reported previously in BSCCO single crystals [6, 16]. Comparison of the dislocation networks in our samples with those reported by other authors and observed at the thin edges of freshly cleaved crystals (i.e. without ion-milling) encouraged us to conclude that the dislocation networks were initially present in our crystals and were not the result of damage by the ion-milling. Figure 3(a) shows an irregular dislocation network observed together with the vortex pattern in sample A. All the dislocations in the micrograph are dissociated into partials joined by stacking faults. This is generally the case in BSCCO [6, 16] owing to its layered crystal structure which leads to a low stacking fault energy. Using $\boldsymbol{g} \cdot \boldsymbol{b}_B$ and $\boldsymbol{g} \cdot \boldsymbol{b}_B \times \boldsymbol{u}$ analyses, the Burgers vectors of the majority of dislocations in figure 3(a) were found to be of $\frac{1}{2}[110] + \frac{1}{2}[110] = [110]$ type, similar to the analysis of reference [6]. Here $\boldsymbol{g}$ is the diffraction vector, $\boldsymbol{b}_B$ is the Burgers vector and $\boldsymbol{u}$ is the unit vector in the direction of a dislocation line. Two dissociated dislocations of this type are marked by filled circles in the micrograph (in the following we shall refer to these dislocations as type I). For dissociated dislocations, which we shall refer to as type II (one of these is marked by an open circle in figure 3(a)), the Burgers vectors were of $\frac{1}{2}[110] + \frac{1}{2}[1\bar{1}0] = [100]$ type. Note that the dislocations of type II have not been previously reported. Both type I and II dislocations lie in the (ab) basal plane making the vortex–dislocation geometry well-defined; that is, the dislocations were always perpendicular to the vortices. For the analysis of vortex–dislocation interactions, the character of the dislocations (screw or edge) determined by the angle between $\boldsymbol{b}_B$ and $\boldsymbol{u}$ is important. In the case of the particular example of type II dislocations in figure 3(a) the dislocations are composed of a pure screw and a pure edge partial. For the dislocations of type I, both partials have the same Burgers vector and the same character. Most of these are of mixed character, i.e. having both screw and edge components, but some are pure screw. Figures 4(a) and 4(b) show two slightly different areas with a degree of overlap of a dislocation system in sample B. Figure 4(a) was taken with the crystal oriented very close to the 200 Bragg condition; figure 4(b) was taken at a deviation from the exact Bragg condition giving optimum dislocation contrast. Therefore, the same dislocations do not give exactly the same contrast in the two micrographs. In sample B (figure 4), one finds the same two types of dissociated dislocations as in sample A (they look somewhat different from figure 3(a) because of the different diffraction vector

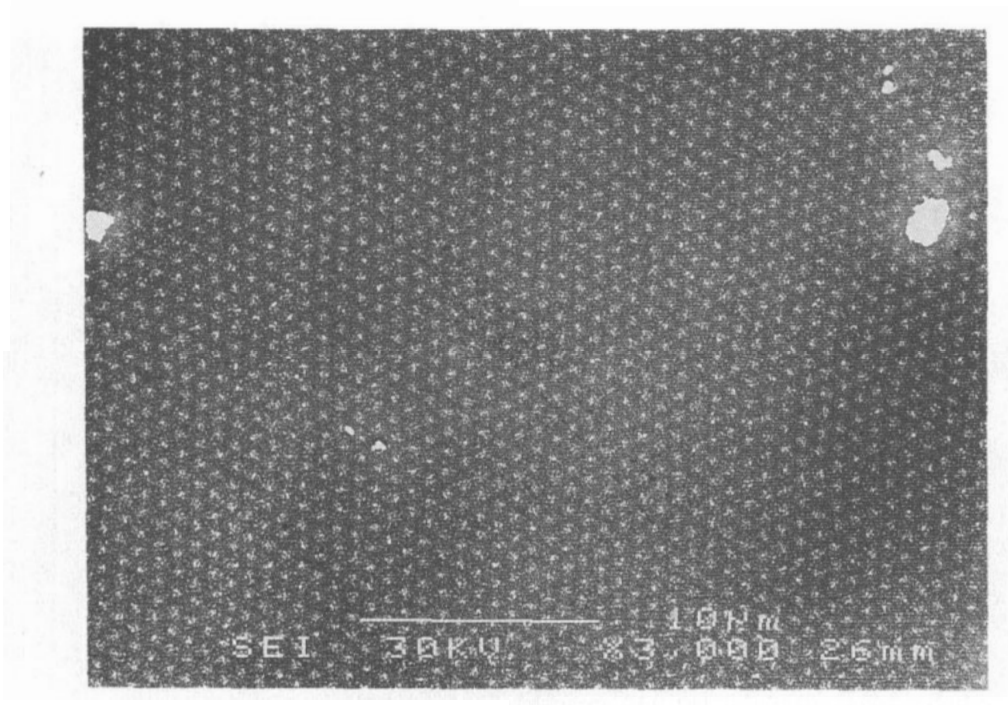

Figure 1. SEM image of the FLL typical for both crystal A and crystal B.

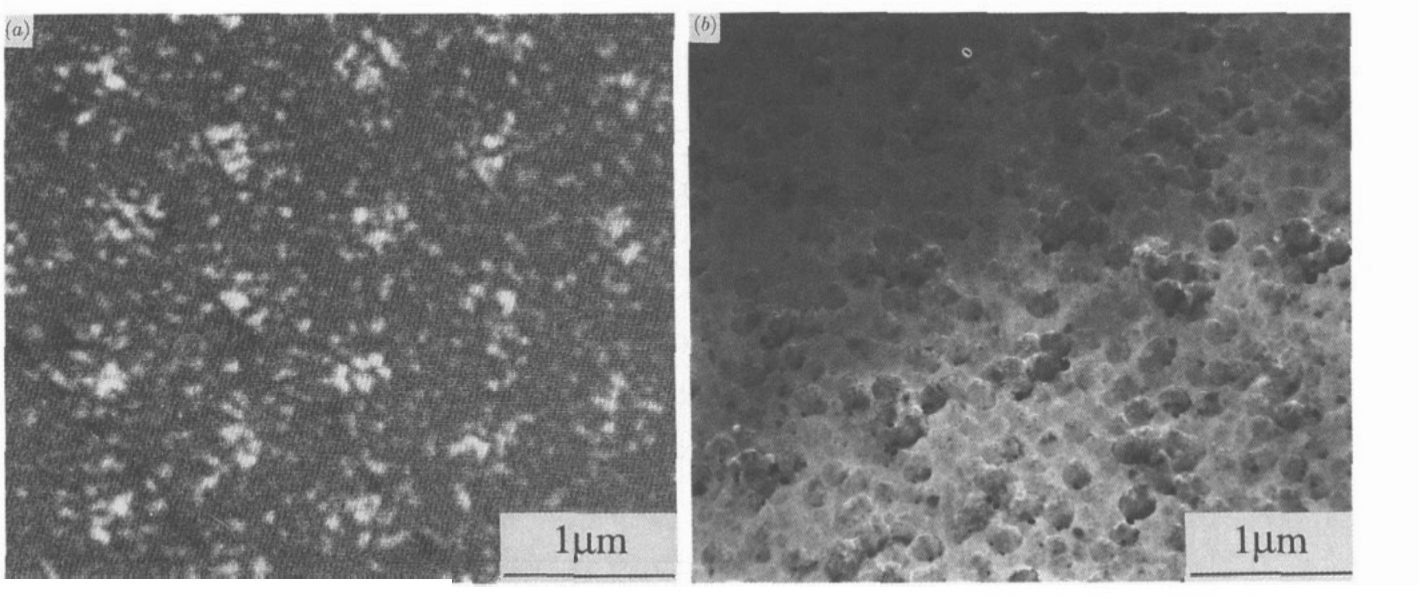

Figure 2. (*a*) SEM image of the FLL in sample A before the carbon film deposition; (*b*) TEM image of the FLL in the same sample, with the carbon film in place.

used to obtain the micrographs). For the most dislocated part of this region, we find long parallel dislocations some of which form closely spaced dislocation pairs. All of these long dislocations have mixed character; for example, in figure 4(*a*) they change from pure screw at the left side to pure edge near the right border of the micrograph. A network of densely spaced dislocations can also be seen in the top left corner of figure 4(*a*).

Let us now turn to the analysis of the effect of dislocations on the vortex arrangement. First of all, the tendency of vortices to align with the dislocations indicates an attractive interaction between them. This interaction causes displacements of the vortices from their equilibrium positions in the FLL that, in turn, create local disorder in the FLL. This order–disorder transformation could be seen clearly when we studied large areas of the FLL, with and without underlying crystal dislocations. Unfortunately, the large magnifications that we had to use for TEM (because of specimen curvature) did not allow us to demonstrate this effect on one micrograph. Nevertheless, one gets an idea of the rapid vortex ordering into a lattice in a dislocation-free area from figure 3(*b*) which shows the vortex positions in figure 3(*a*). Apart from the presence of one FLL dislocation which is indicated by the arrow, the vortex lattice in the defect-free part of figure 3(*a*) is essentially regular. Its regularity was more obvious when large areas of the FLL

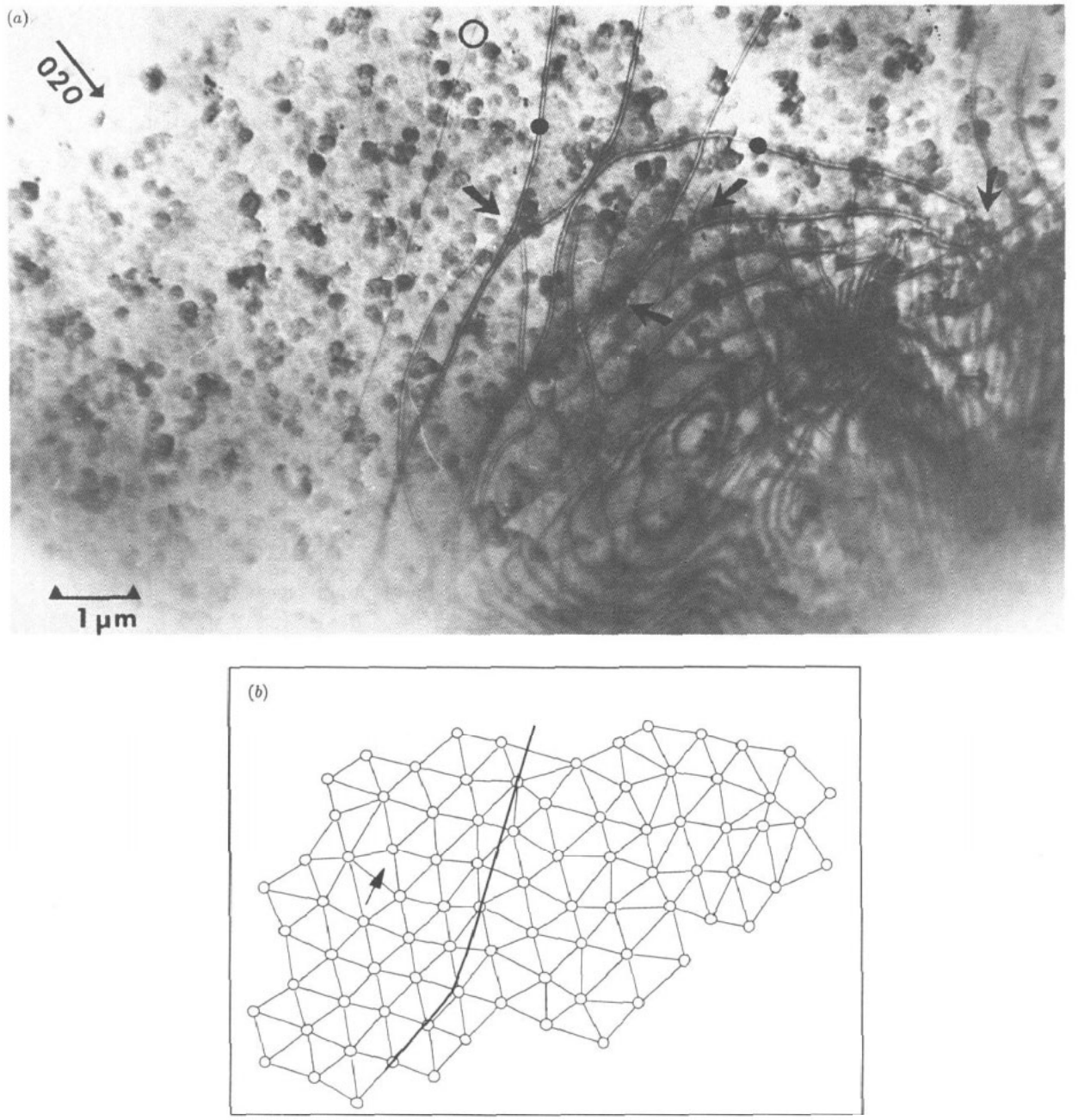

Figure 3. (*a*) TEM image of the vortex pattern in the vicinity of a dislocation network in sample A. The micrograph is taken using the diffraction vector g = [020]. Filled circles mark two of the type I dislocations; an open circle marks one of the type II dislocations (see text). Arrows indicate locations of dislocation intersections where vortices are trapped. (*b*) Computerized vortex positions and bonding of the vortex arrangement in (*a*). The solid line shows a position of the first-from-the-left dislocation of the dislocation network in (*a*). The arrow shows a defect (edge dislocation) in the FLL.

further to the left of the micrograph (not shown) were examined. At the same time, the presence of dislocations always caused vortex displacements from regular positions in the FLL as described above and as one can also see from figure 3(*b*). Note that on going from the disordered vortex arrangement in the dislocated area to the defect-free region, the FLL order is restored very quickly, over the distance of the order of one vortex period, a. This indicates that the effect of dislocations on the FLL, although substantial, is very local, i.e. restricted to the area where there are dislocations. In other words, this means that the vortex–dislocation interaction has a short pinning range, r_p, of the order of or smaller than the average vortex spacing (at least, it is true for low magnetic fields used in our experiments). Another important feature obvious in all three micrographs is that the vortex–dislocation attraction does not depend on the nature of the dislocations (screw or edge). Furthermore, in the parts of the crystals where the dislocations form networks (most of the dislocation system in figure 3(*a*) and also top left part of figure 4(*a*)),

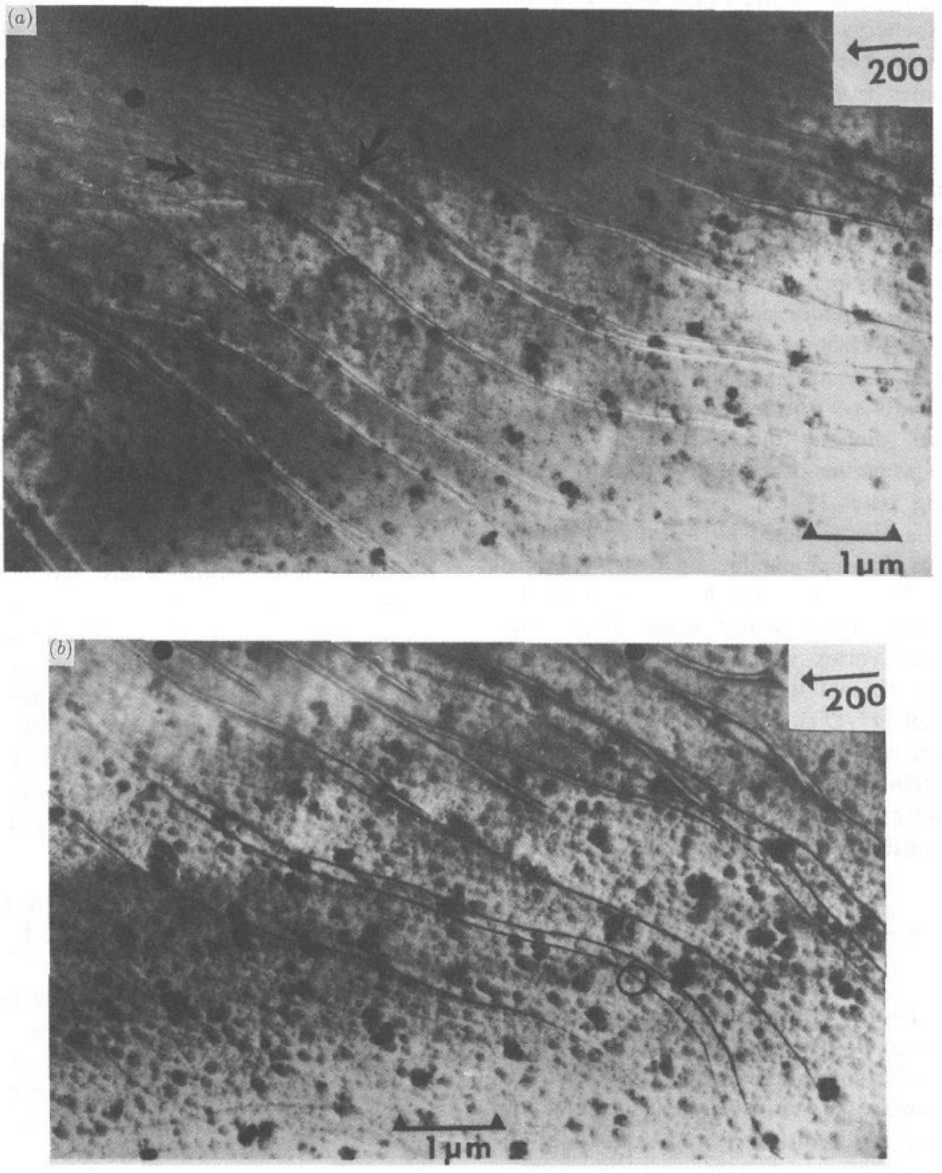

Figure 4. (*a,b*). TEM images of the vortex–dislocation arrangements in sample B. Both micrographs are taken using $g \approx [200]$ diffraction vector but under slightly different Bragg conditions (see text). Filled circles mark some of the dislocations of type I. An open circle marks a dislocation of type II (see text). Arrows indicate the vortices captured at the dislocation intersections.

the vortices are preferentially captured by the dislocation intersections (some of these captured vortices are marked by arrows in the photographs). Where the spacings of the intersections, D, scale approximately with the vortex spacing, matching pinning [1] is observed, i.e. every intersection is occupied by a vortex for $D \geq a$ or every vortex sits at the intersection for $D < a$. In the central part of figure 3(*a*), the condition $D > a$ is valid and the above matching effect leads to a small, $\approx 15\%$, increase in the local vortex spacings. On average, however, the distance between the vortices in dislocation-affected areas of the vortex lattice is the same as in the undisturbed FLL in the defect-free parts of the crystals.

3. Discussion

Theoretically, three different mechanisms were proposed for the vortex–dislocation interaction. The first is due to a local suppression of the vortex energy by the strain fields around a dislocation [9, 17]. Regions of severe strain can lead to a significant reduction of the electron mean free path that will result in changes of superconducting parameters such as a decrease of ξ and an increase of λ and the Ginzburg–Landau (GL) parameter, $\kappa = \lambda/\xi$ [18]. Then, the vortex–dislocation interaction energy will be proportional to a resultant change of the vortex energy

$$J = \left(\frac{\Phi_0}{4\pi\lambda}\right)^2 \ln\kappa + \left(\frac{H_c^2}{8\pi}\right)\pi\xi^2.$$

Here H_c is the thermodynamic critical field and the second term in the vortex energy represents the energy of the normal core. The main contribution to electron scattering by dislocations comes from the long-range strain fields rather than from the dislocation cores [19] (the latter represent regions, ~2–3 b_B in size, of a severely distorted crystal). Therefore, the variations of the vortex-free energy can be substantial even if the condensation energy, $H_c^2/8\pi$, remaines unchanged, i.e. well away from the dislocation cores. For high-temperature superconductors which have very short ξ values, an additional contribution, due to suppression of the condensation energy in the vicinity of the dislocation cores, may also become important. This type of interaction is always *attractive*.

The other two pinning mechanisms arise from variations of elastic properties of materials between normal and superconducting states [9–13]. Since the core of a vortex, in general, is characterized by a different atomic volume from that of the superconducting matrix (typical differences are $\sim 10^{-7}$), a vortex behaves as an elastic inclusion and gives rise to a permanent elastic stress field. The dilatation in the vortex state, $\delta\varepsilon_v(r)$, depends on the order parameter, so that it can be approximated by $\delta\varepsilon_v(r) = \delta\varepsilon_{v0}[1-\exp(-r^2/\xi^2)]$, where $\delta\varepsilon_{v0}$ is the dilatation in the Meissner state with respect to the normal state [1]. For a tetragonal system and a straight vortex perpendicular to the layers, the stress tensor associated with the vortex at $r \gg \xi$ is (in cylindrical coordinates) [1, 10]

$$\sigma = \frac{A\xi^2}{r^2}\begin{bmatrix} 1 & 0 & 0 \\ 0 & -1 & 0 \\ 0 & 0 & 0 \end{bmatrix} \tag{1}$$

where $A = -\delta\varepsilon_{v0}\mu(1+\nu)/3(1-\nu)$, μ is the shear modulus of the crystal and ν is Poisson's ratio. This stress field interacts with the dilatational stresses that exist around dislocations. The interaction energy is linear in the defect stress field and, therefore, is often referred to as the first-order (paraelastic) interaction. A resultant pinning force per unit length is [10]

$$F = -\sigma \cdot b_B \times \mathrm{d}l \tag{2}$$

where σ is the stress tensor of the vortex, b_B is the Burgers vector of the dislocation and $\mathrm{d}l$ is a unit vector along the dislocation. This type of interaction does not exist for screw dislocations because they have no associated dilatation and produce only shear stress so that $b_B \times \mathrm{d}l = 0$ in equation (2) and F is zero. For an edge dislocation, the sign and magnitude of the interaction force depend on the geometrical arrangement between the vortex, the dislocation and its Burgers vector.

(i) For an edge dislocation parallel to a vortex there is a net *attractive* force which is at a maximum for a distance between the vortex and the dislocation of the order of the coherence length, ξ.

(ii) For an edge dislocation perpendicular to a vortex and its Burgers vector parallel to it, the interaction produces local torque forces at distances $r \ll \xi$ and is vanishingly small at $r \gg \xi$.

(iii) For both the edge dislocation and its Burgers vector perpendicular to a vortex, the first-order interaction produces local torque forces on the dislocation while the vortex is attracted to the compressed region of the dislocation and repelled from its expanded region. For $r \gg \xi$, the interaction force is vanishingly small.

The second-order (dielastic) interaction arises from a small (10^{-4}–10^{-5}) change of elastic moduli of the material on passing from the normal to the superconducting state [12, 13]. For conventional superconductors like Pb, V or Nb, it has been established from temperature-dependent sound velocity measurements [20, 21] that the materials are elastically softer in the superconducting state. At low temperatures, the elastic constants measured in zero magnetic field (i.e. when the material is superconducting) are always smaller than those measured in a magnetic field $H > H_{c2}$ [20]. Then, in the presence of vortices a superconductor behaves as an elastically inhomogeneous medium: it is stiffer where the normal cores of the vortices are situated. As a result, the self-energy of defects (dislocations, in particular) is higher in the vicinity of the vortex cores. This type of interaction is always *repulsive* and should exist both for screw and edge dislocations. Unlike the first-order interaction, it does not depend on the orientation of the Burgers vector relative to the orientation of a vortex. The pinning force per unit length exerted on a vortex from a perpendicular screw dislocation a distance r away from it, is

$$f_p = -\Delta S_{44}\left(\frac{b_B^2}{4\pi}\right)\frac{\xi^2}{r^2} \tag{3}$$

where ΔS_{44} is the difference in shear modulus between the normal and superconducting regions. For a vortex and a parallel screw dislocation, f_p falls off as $1/r^3$. In both cases the force is at a maximum for the distance between a vortex and a dislocation $r \approx \xi$. For an edge dislocation, the dielastic interaction forces are similar to the forces on a screw dislocation.

Unfortunately, for high-temperature superconductors in general, and BSCCO in particular, there is no direct evidence at present that these materials are also elastically softer in the superconducting state. Measurements similar to those on conventional superconductors are obviously very difficult to make because of the extremely high values of the upper critical field, H_{c2}. Elastic softening associated with the superconducting transition (against the overall increase of elastic moduli with decreasing temperature) was observed both for YBCO [22] and BSCCO [23, 24], similar to conventional superconductors. However, a number of additional new features were also found, such as a substantial increase of the stiffening rate below T_c for YBCO [25] or several softening minima above T_c for BSCCO [24]. Although these experimental results, by themselves, are not in conflict with the superconducting state being elastically softer than the normal state, direct measurements of elastic moduli with and without magnetic field are desirable to clarify the situation.

In the following we shall assume that, similar to conventional superconductors, normal cores of the vortices

in BSCCO are characterized by larger elastic moduli. Then, if elastic vortex–dislocation interactions are important, one should expect the interaction sign either to be different for screw and edge dislocations, or to be always repulsive (if the dominant contribution comes from the dielastic interaction). The pinning strength in this case should also depend on the character of a dislocation, its orientation relative to the vortex and its Burgers vector. In experiment, however, we observe that all dislocations—screw, edge and mixed—have similar effects on the vortex structure and, moreover, the pinning force is always attractive. Furthermore, there are clear indications that the strongest pinning is produced by regions characterized by a local increase in the dislocation strain field. For example, if there is a pair of two closely spaced dislocations of the same sign, the strain field components are the largest in between the two dislocations [26] and this is where we always observe trapped vortices (see figure 4). Furthermore, dislocation intersections that, as a rule, also represent places of local enhancement of the elastic strain field, are clearly the strongest pinning centres observed in the experiment. In general, calculations of the strain fields around dislocation intersections is rather complicated. However, our point can be qualitatively illustrated by three dislocation intersections shown in figure 5. At the site marked 1, two dissociated dislocations come together: one of them, of type II (weaker contrast and narrower image), consists of a pure edge and a pure screw partial; the other, of type I, is mixed. In addition, the two dislocations have the same sign and, therefore, strongly interact with each other producing a local enhancement of the strain field. This site has captured a vortex. At the site marked 2, two dislocations of the opposite signs intersect: one of them (vertical) is screw while the other is almost pure edge so that there is virtually no interaction between them [26]. There is no enhancement of the strain field and no vortex at this site. At site 3, where there is a captured vortex, three dislocations come together. Two of them have the opposite signs and are nearly parallel, with considerable reduction of long-range strain energy. The third, visible only in the lower half of the micrograph and terminating at the region of intersection, is evidently close to one of the specimen surfaces. The net stress at the decorated surface cannot be estimated without knowledge of the relative depths of the three dislocations within the specimen. However, it is clear that the third dislocation has the same sign of the Burgers vector as one of the two dislocations that are continuous through the intersection. Everything taken into account, one should expect local enhancement of the strain field at site 3, too.

We conclude from our observations and the above consideration that in the presence of dislocation networks, dominant pinning arises from the places of local enhancement of the strain field. Contributions from the elastic interactions, although they must also be present, are apparently weaker and do not have any noticeable effect on the vortex arrangement. This indicates that in our case (low magnetic fields, where the vortex–vortex interaction is exponentially weak; all dislocations perpendicular to the vortices; typical distances between the dislocations are comparable with the vortex spacing) the dominant pinning

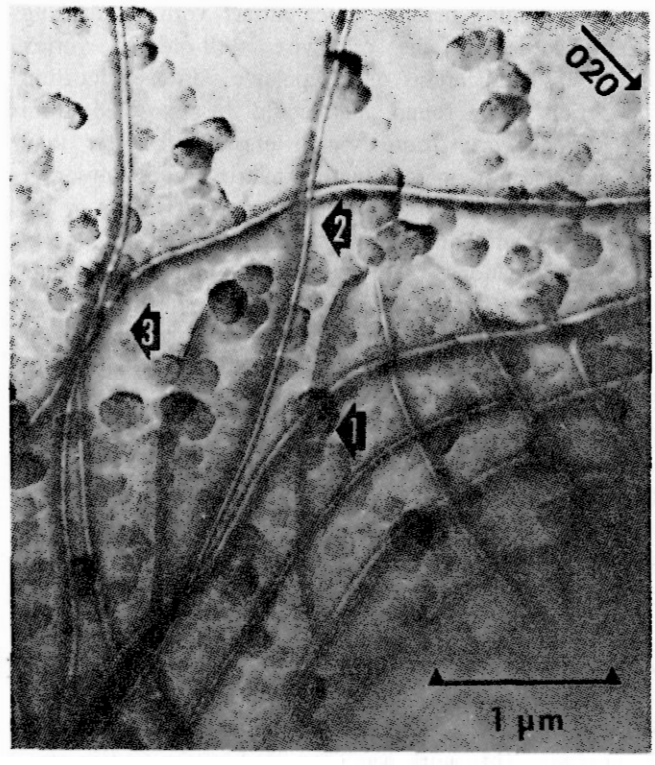

Figure 5. A small part of the TEM image of figure 3(*a*) showing several types of dislocation intersections.

mechanism is most likely to arise from the local changes of ξ, λ and κ, owing to the dislocation strain fields. The importance of the strain fields, rather than the dislocations themselves, for suppression of the superconductivity and the critical currents was also suggested by a recent study of the critical currents against grain boundary misorientation angle in YBCO thin films [17].

It is interesting to note that in earlier experiments on single crystals of a conventional superconductor, NbMo ($\xi \approx 300$ Å), clear indications of a repulsive second-order interaction between the vortices and parallel screw dislocations were observed [3]. It is possible that a very short coherence length in BSCCO and hence a very small volume fraction occupied by the vortex cores makes the dielastic interaction unimportant, at least in low magnetic fields. As to the paraelastic interaction, no definitive conclusions can be drawn from our experiment because of the perpendicular vortex–dislocation geometry. As discussed above, in such a case one can expect only negligibly small forces on the vortices at distances $r \gg \xi$ [10].

4. Conclusions

A technique allowing simultaneous observation of the vortex images and dislocations by transmission electron microscopy has been developed. The technique, which includes the Bitter decoration method as a means for visualization of the vortex arrangement, was used to study vortex pinning by crystal dislocations in high-quality as-grown single crystals of BSCCO-2212. Our experiments demonstrate that dislocations in BSCCO are

effective pinning centres which attract vortices, causing local disorder in the otherwise well-ordered vortex lattice. No indications of a repulsive vortex–dislocation interaction were found that could be expected from the normal vortex cores being elastically stiffer than the surrounding superconducting matrix (second-order or dielastic interaction). The most important factor in the vortex–dislocation interaction is found to be the strain fields around dislocations. The strongest pinning forces come from the most strained regions of the crystal that, in our crystals, are intersections of the dislocations and pairs of closely spaced dislocations of the same sign and character. From these we conclude that the dominant mechanism of pinning is most likely to arise from the local suppression of vortex energy due to the strain fields around dislocations. Our observations suggest that the introduction of regular dislocation networks into layered superconducting materials should be an effective way of enhancing bulk pinning and critical currents, due to matching pinning effects.

Acknowledgments

We wish to thank C E Gough and V G Kogan for helpful discussions. This work was supported by the Engineering and Physical Sciences Research Council of the United Kingdom.

References

[1] Campbell A M and Evetts J E 1972 *Adv. Phys.* **21** 191
[2] Herring C P 1976 *J. Phys. F: Met. Phys.* **6** 99
[3] Grigorieva I V and Vinnikov L Ya 1989 *J. Low-Temp. Phys.* **74** 81
Grigorieva I V 1989 *Sov. Phys.–JETP* **69** 194
[4] Selvamanickam V, Mironova M, Son S and Salama K 1993 *Physica* C **208** 238
[5] Zheng X, Nishioka S, Kuriyaki H and Hirakawa K 1994 *Japan. J. Appl. Phys.* **33** 1309
[6] Yang G, Shang P, Sutton S D, Jones I P, Abell J S and Gough C E 1993 *Phys. Rev.* B **48** 4054
Shang P, Yang G, Jones I P, Gough C E and Abell J S 1993 *Appl. Phys. Lett.* **63** 827
[7] Miller D J, Sengupta S, Hettinger J D, Shi D, Gray K E, Nash A S and Goretta K C 1992 *Appl. Phys. Lett.* **61** 2823
[8] Liu H K, Guo Y C and Dou S X 1992 *Supercond. Sci. Technol.* **5** 591
[9] Narlikar A V and Dew-Hughes D 1964 *Phys. Status Solidi* **6** 383
[10] Kramer E J and Bauer C L 1967 *Phil. Mag.* **15** 1189
[11] Kronmüller H and Schmucker R 1973 *Phys. Status Solidi* b **57** 667
Schneider E and Kronmüller H 1976 *Phys. Status Solidi* b **74** 261
[12] Webb W W 1963 *Phys. Rev. Lett.* **11** 191
[13] Schneider E 1978 *J. Low-Temp. Phys.* **31** 357; 1978 *J. Low-Temp. Phys.* **31** 357
[14] Balakrishnan G, Paul D McK, Lees M R and Boothroyd A T 1993 *Physica* C **206** 148
[15] Li T W, Kes P H, Hien N T, Franse J J M and Menovsky A A 1993 *J. Cryst. Growth* **130** 411
[16] Song C, Liu F, Gu H, Lin T, Zhang J, Xiong G and Yin D 1991 *J. Mater. Sci.* **26** 11
Li Z, Shen H, Qin Y, Jiang J and Du J 1989 *Phil. Mag. Lett.* **60** 123
[17] Chisholm M F and Penneycook S J 1991 *Nature* **351** 47
[18] Tinkham M 1975 *Introduction to Superconductivity* (New York: McGraw-Hill)
[19] Gantmakher V F and Levinson I B 1984 *Scattering of Current Carriers in Metals and Semiconductors* (Moscow: Nauka) ch 10 (in Russian)
[20] Alers G A and Waldorf D L 1961 *Phys. Rev. Lett.* **6** 677
[21] Rayne J A and Chandrasekhar B S 1960 *Phys. Rev.* **120** 1658
[22] Hoen S, Bourne L C, Choon M K and Zettl A 1988 *Phys. Rev.* B **38** 11949
[23] Boekholt M, Harzer J V, Hillebrands B and Güntherodt G 1991 *Physica* C **179** 101
[24] Wu J, Wang Y, Guo P, Shen H, Yan Y and Zhao Z 1993 *Phys. Rev.* B **47** 2806
[25] Bishop D J, Ramirez A P, Gammel P L, Batlogg B, Rietman E A, Cava R J and Millis A J 1987 *Phys. Rev.* B **36** 2408
[26] Hirth J P and Lothe J 1968 *Theory of Dislocations* (New York: McGraw-Hill)